

# Paper Substrate Classification based on 3D Surface Micro-geometry

Hossein Malekmohamadi<sup>1</sup>, Khemraj Emrith<sup>2</sup>, Stephen Pollard<sup>1</sup>, Guy Adams<sup>1</sup>, Melvyn Smith<sup>2</sup>  
and Steve Simske<sup>1</sup>

<sup>1</sup>*Printing and Content Delivery Lab, Hewlett Packard Laboratories, Bristol, U.K.*

<sup>2</sup>*Machine Vision Laboratory, University of the West England, Bristol, U.K.*

**Keywords:** Photometric Stereo, Shape index, Co-occurrence Matrices, Paper Classification.

**Abstract:** This paper presents an approach to derive a novel 3D signature based on the micro-geometry of paper surfaces so as to uniquely characterise and classify different paper substrates. This procedure is extremely important to confront different conducts of tampering valuable documents. We use a 4-light source photometric stereo (PS) method to recover dense 3D geometry of paper surfaces captured using an ultra-high resolution sensing device. We derived a unique signature for each paper type based on the shape index (SI) map generated from the surface normals of the 3D data. We show that the proposed signature can robustly and accurately classify paper substrates with different physical properties and different surface textures. Additionally, we present results demonstrating that our classification model using the 3D signature performs significantly better as compared to the use of conventional 2D image based descriptors extracted from both printed and non-printed paper surfaces. Accuracy of the proposed method is validated over a dataset comprising of 21 printed and 22 non-printed paper types and a measure of classification success of over 92% is achieved in both cases (92.5% for printed surfaces and 96% for the non-printed ones).

## 1 INTRODUCTION

Counterfeit of valuable documents is growing at a gigantic scale, mainly due to the rapid evolution of modern printing technologies. Existing document security systems are unable to meet the requirements for document security in terms of accuracy and robustness prompting the need for more advanced, but cost-effective methods to verify the authenticity and originality of print documents. The early stage to protect valuable print documents is to recognise paper type.

Traditional methods (Chiang et al., 2009; Khanna and Delp, 2010) to secure print documents use 2D details of recorded digital images. However, recent developments in fraud tampering make the job of print security even tougher. Recent improvements in extracting robust features for print inspection have looked at acquiring high resolution 2D images of printed materials for better feature extraction and representation (Chiang et al., 2009). However with paper surfaces being inherently isotropic with significantly fine random details, the inspection or classification systems based on 2D features has so far proved to be considerably inaccurate. This can be mainly attributed to the fact that direction of illumination has

a filtering effect which removes structural information along the illumination direction (Chantler et al., 2005). Additionally, studies using 2D features capture only variations in intensity of surfaces and fail to capture the surface height variations, i.e. the 3D texture of surfaces being analysed (Cula and Dana, 2001; McDaniel and Panchanathan, 2007).

For more precise paper substrate (printed and non-printed) characterisation 3D surface representations have been investigated. For example in (Buchanan et al., 2005), Buchanan et al used a laser microscope to image paper texture. While the system is able to capture the 3D surface scattering, it is expensive and cannot be widely applied. Clarkson et al (Clarkson et al., 2009) used commodity scanners to capture 2D blank paper fingerprints and use the Photometric Stereo (PS) method to extract 3D surface information. Although relatively cheap, this method lacks in robustness and accuracy that arises from the inadequate resolution of the scanners and the uncontrolled directional lights from the scanners.

To capture and model the surfaces of print materials at micro-structure level, ultra-high resolution techniques have been studied. In (Adams, 2010), a new device to record 2D images of print in fine details is

introduced. Johnson et al (Johnson et al., 2011) employed elastomeric sensor to acquire images which are later used by a PS algorithm to extract micro-geometry of different surfaces. A 3-light source PS system is used by Kuperinen et al (Kuperinen et al., 2007) to extract paper surface topography. However, none of these studies have provided a practical solution to develop a robust and secure system to identify different paper types.

In this work we provide a model to classify paper types using a novel signature that is based on the fine 3D structural information of paper materials. Using a 4-light source PS method and microscopic photometric images captured from a high resolution sensing device we generate 3D surface texture at a microstructure level. We derive a novel 3D signature based on the shape index (SI) map computed from the surface normals. We show that different paper types can be classified accurately, despite the presence of print parasitics, meeting the requirements for forensic paper inspection.

## 2 PHOTOMETRIC STEREO

To recover highly dense surface information, we employ the PS technique which is based on high-resolution image acquisition using a number of different light source directions and a single camera. PS is used to estimate the dense normal map of a scene, from which the gradient field is then computed. This enables robust separation of the 2D (albedo) and 3D (bump map) components of the scene at a significantly high level of accuracy.

PS has been available for many decades (Woodham, 1980) but only recently has affordable technology become available for improving camera resolution and algorithm execution speed, allowing synchronised light switching at the fast rates needed to avoid inter-frame motion. We use 4 photometric images (4 source PS system) to recover the 3D surface information from papers (blank or with glyph). While fewer photometric images could be sufficient, a 4 source PS system allows better recovery in the presence of highlights and shadows (Barsky and Petrou, 2003). We assume a Lambertian reflectance model together with intensity variation at each pixel to estimate local surface orientations. The integration of these surface orientations results in a highly detailed estimate of the surface geometry.

Figure 1 shows the set-up for the capture of photometric images.  $\tau$  denotes tilt angle and represents the angle that an illuminant vector projected onto the surface plane makes with  $x$ -axis. The slant angle,  $\sigma$ ,

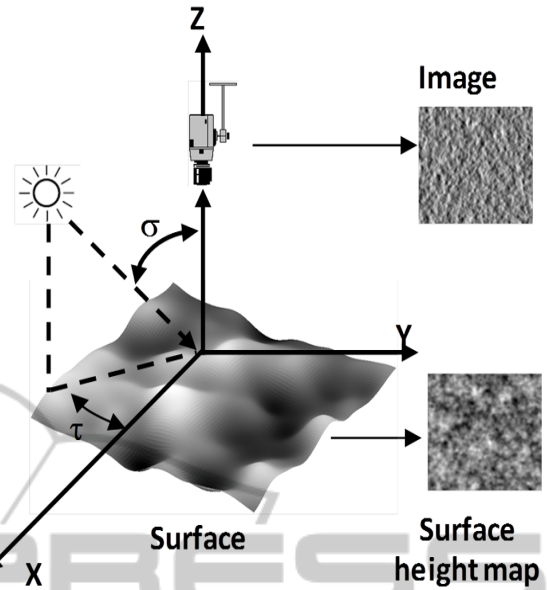


Figure 1: Set-up for capturing images in PS algorithm.

represents the angle the illuminant vector makes with the  $z$ -axis. The function to represent the photometric images at individual illumination direction is as follows:

$$i(x,y) = \frac{-p(x,y)\cos\tau\sin\delta - q(x,y)\sin\tau\cos\delta + \cos\delta}{\sqrt{p(x,y)^2 + q(x,y)^2 + 1}} \quad (1)$$

It is important that the three photometric images provide enough change in illumination gradient so that the partial derivatives for the surface ( $p$  and  $q$ ) can be estimated. Based on the assumption that Lambert's law is preserved, we model that reflectance functions for the 4 PS images as

$$i_d(x,y) = \rho(l_d n) \quad \forall d \in \{1,2,3,4\} \quad (2)$$

With known reflectance intensities  $i_d$  and illumination directions  $l_d$  (which are fixed in the camera coordinate), the unit surface normal at a given position  $(x,y)$  in the surface plane is given by  $n = \frac{(p,q,-1)^T}{\sqrt{p^2+q^2+1}}$  with  $p$  and  $q$  being the partial surface derivatives.

## 3 EXPERIMENTAL SETUP

This section describes our photometric image capture process and the generation of 3D surface datasets for (non-) printed paper substrates.

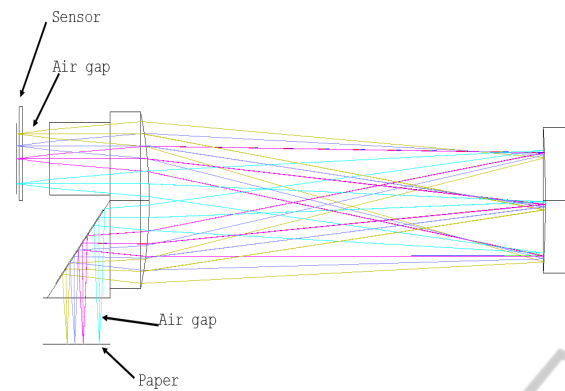


Figure 2: Imaging device.

### 3.1 Imaging Device

In this paper, we employ a similar device to (Adams, 2010; Simske and Adams, 2010) to capture the photometric images. Our device is capable of resolving spatial features of less than 5 microns with 1:1 magnification. Just as in the case of (Adams, 2010; Simske and Adams, 2010) we also use a single Dyson relay lens in series with a mirror and a low cost 3.2 m/pixel, 3 MP CMOS colour image sensor. However, we have adapted our device for the current study by modifying its design to accommodate a 4.5mm air-gap for the paper and for the sensor as shown in Figure 2. This gap enables light to be projected from multiple sources and from a range slant angles. The sensor air gap needs to be symmetrical due to the inherent relay properties of the lens operation i.e. the input and output paths to/from the mirror.

Theoretical resolution of the lens design over a field of view (FOV) of 4.8mm is approximately 8800lpi (30% MTF (modulation transfer function)). In practice with manufacturing and assembly tolerances this reduces to nearer 7000lpi. Figure 3 shows that MTF at the diffraction limit (346 lines per mm = 173 cycles/mm) and over the full FOV is approximately 0.4 which would result in satisfactory image contrast. Due to the existing air gap, ambient illumination effects need proper consideration. An image is captured with all LEDs off to record ambient illumination profile. Afterwards, this image is cancelled out from captured images with LEDs on. The resultant imaging device is shown in Figure 4.

### 3.2 3D Paper Surface Dataset

We generated an initial dataset with images captured from a set of 22 different paper types. For every paper type we captured photometric images from 12 random locations. As a result the first dataset comprised of a

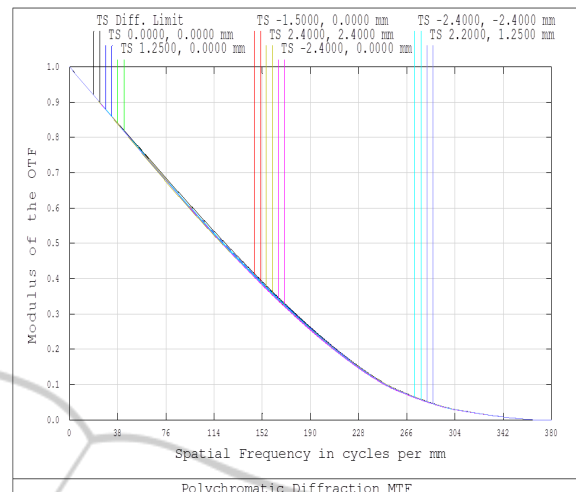
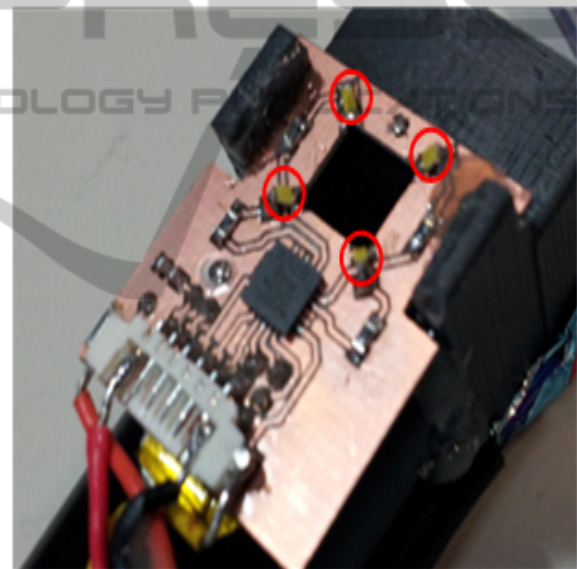
Figure 3: Simulated MTF over  $5 \times 5$ mm FOV.

Figure 4: An image of the device looking into the optics (i.e. device is upside down). Image sensor and white LEDs are assembled into a custom built, 3D printed frame.

total of 264 (i.e.  $12 \times 22$ ) 3D surfaces.

To generate the dataset for printed surfaces, we used a checkerboard pattern that was printed at 12 random locations of a set of 21 different paper types (one ignored because of its thickness) leading to a set of 252 3D surfaces. A laser printer was used in this process.

Photometric images of size  $1024 \times 1024$  pixels were used to recover each 3D surface. Figure 5 shows the rendered 3D surface of the same paper type from the two different sets. Frankot & Chellappa's method (Frankot and Chellappa, 1988) was used to integrate the partial derivatives of the surfaces. This is done

solely for visualisation purposes since we use only the surface normals for feature extraction. Through visual inspection we can identify the micro-geometry of both the printed and non-printed regions.

#### 4 3D SIGNATURE EXTRACTION

For the feature extraction stage, we use the partial derivatives of the 3D surfaces  $(p, q)$  to extract surface curvature information. We compute the first order derivatives along the  $x$ -axis and  $y$ -axis for  $p$  and  $q$ :  $p_x$ ,  $q_y$ ,  $p_y$ . These derivatives are used to compute the surface curvature. The Gaussian curvature,  $K$ , is given by

$$K = \frac{p_x q_y - p_y^2}{(1 + p^2 + q^2)^2} \quad (3)$$

Mean curvature is

$$H = \frac{(1 + p^2)q_y + (1 + q^2)p_x - 2pqp_y}{2(1 + p^2 + q^2)^{\frac{3}{2}}} \quad (4)$$

The principle curvatures  $k_{1,2}$  are

$$k_{1,2} = H \pm \sqrt{H^2 - K} \quad (5)$$

The resultant principal curvatures are used to compute a shape index (SI) map for each 3D surface. This provides a characterisation of topography using a continuous angular representation (Koenderink and van Doorn, 1992). Shape index is defined as

$$S = \frac{2}{\pi} \arctan\left(\frac{k_2 + k_1}{k_2 - k_1}\right) \quad (6)$$

In Figure 6 we illustrate the shape index maps of two surface patches extracted from same paper type taken from dataset 1 and 2 respectively. The shape index maps presented appear to be able to capture significant amount of 3D surface texture information in both the printed and non-printed surface patches of the paper type selected. More importantly, from the shape index map of the printed paper (Figure 6 (bottom)) we can clearly see that the texture information of the non-printed region is preserved together with the texture information of the printed region being considerably different.

The features used in the classification of the different paper types are obtained by extracting co-occurrence information from the SI maps. These matrices are computed using the local neighbourhood of every SI map element (pixel) in the horizontal and vertical directions (Haralick et al., 1973). Among the

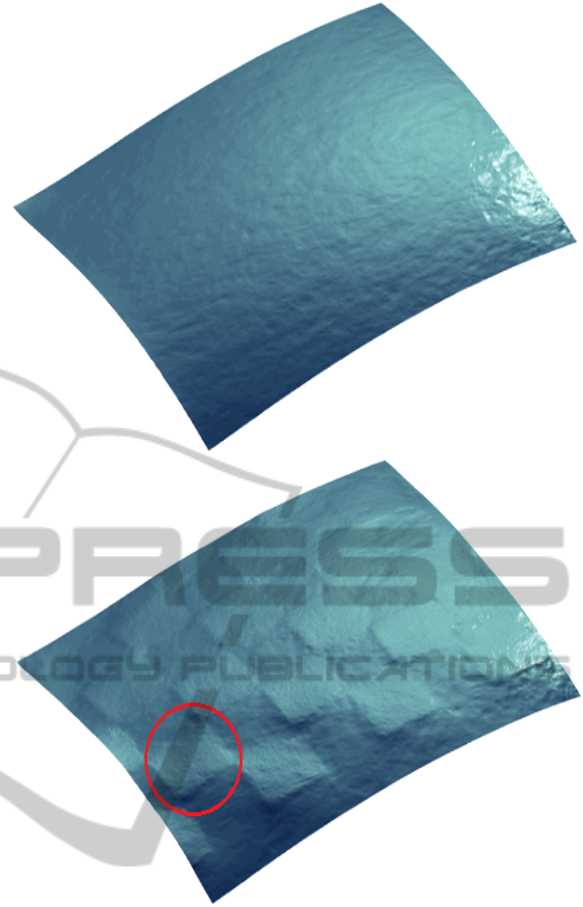


Figure 5: Surface for a blank paper (top) and the same paper with printed stimuli (bottom): for better visualisation, one example of printed region is marked in red.

co-occurrence features, contrast and energy measures are used in this paper. Contrast ( $\delta$ ) is computed from the co-occurrence matrix ( $G$ ) as follows:

$$\delta = \sum_{i,j} |i - j|^2 G(i, j). \quad (7)$$

Energy ( $\epsilon$ ) is given by

$$\epsilon = \sum_{i,j} G(i, j)^2. \quad (8)$$

Finally, we extract entropy ( $\zeta$ ) for the SI map ( $S$ ) as

$$\zeta = - \sum_{i,j} S \log_2 S \quad (9)$$

Consequently, the features described in Table 1 are extracted for all 3D surfaces from both datasets and are then fed to a classifier.

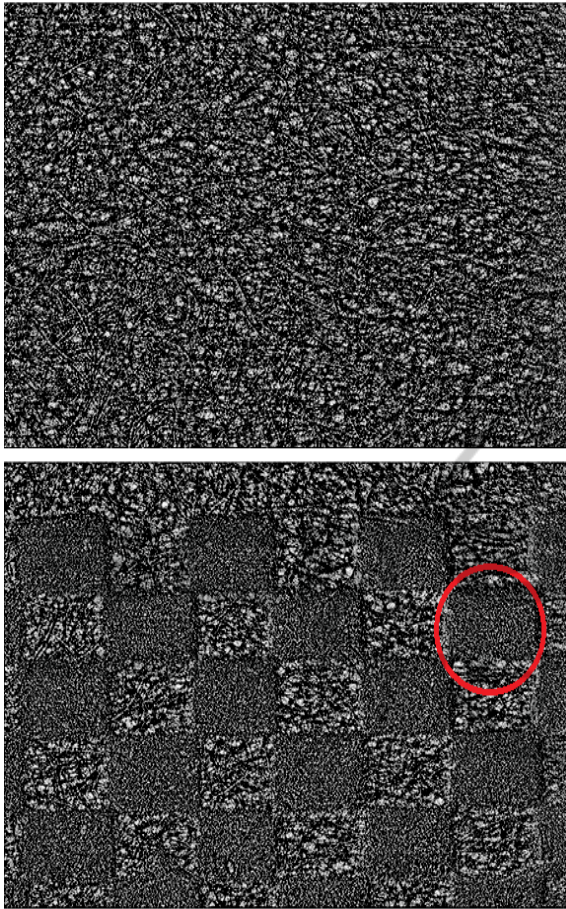


Figure 6: Surface for a blank paper (top) and the same paper with printed stimuli (bottom): for better visualisation, the corresponding SI region to the marked part of the surface (See Figure 5) is circled in red.

Table 1: Set of parameters extracted for the SI map for non-printed and printed datasets.

Parameter	Description
$\delta_H$	Horizontal Contrast for SI
$\delta_V$	Vertical Contrast for SI
$\epsilon_V$	Horizontal Energy for SI
$\epsilon_V$	Vertical Energy for SI
$\zeta$	Entropy for SI

## 5 RESULTS & DISCUSSIONS

A neural network is used to train, validate and test the data set to predict paper types from both datasets. In the first experiment, we train a classifier to categorise the different paper substrates. We use 50% of the overall number of samples from each dataset for training purposes. An additional 15% is used to validate

the neural network to avoid overfitting. The remaining 35% is then used for testing purposes. The neural network training function is based on Levenberg-Marquardt optimisation (Marquardt, 1963). The number of neurons in the hidden layer is 5. To show the improvement in classification from using 2D descriptors, we apply the neural network classifier to features extracted from the albedo map of each paper type. The same features as presented in Table 1 are used.

### 5.1 Blank Paper Classification (Dataset 1)

The results of applying the neural network classifier to dataset 1 are shown in Table 2. Learning stops at epoch 20 when the Mean Squared Error (MSE) for validation data is 5.32. Table 2 shows the results of applying the classifier to the albedo maps. For this scenario, learning stops at epoch 91 when MSE for validation data is 6.73. In the 2D scenario, some paper types are misclassified (test performance is 86.42%) whereas using 3D dense information they are more clearly differentiated (test performance is 95.96%). The reason is that in 2D case, statistical and structural properties of similar paper types have closer values but in the 3D case, similar paper types have more distinctive statistical and structural properties.

Table 2: Classification results with 3D and 2D information for dataset 1.

Feature	Training	Validation	Test
3D	92.33	94.08	95.96
2D	91.91	92.87	86.42

### 5.2 Printed Paper Classification (Dataset 2)

In the case of applying the classifier to dataset 2, learning stops at epoch 7 when MSE for validation data is 4.29. The results for this classifier are shown in Table 3. Learning stops at epoch 37 when MSE for validation data is 6.64. Just as in the case of the results in Section 5.1, using 2D features extracted from the albedo images result in some paper types being misclassified (test performance is 89.36%). When features are extracted from the dense 3D information, the paper types are more clearly differentiated (test performance is 92.55%).

Lower accuracy in the 2D scenario (features applied to the albedo map) for the non-printed dataset is due to the fact that the statistical and structural properties of similar paper types are much closer than in the 3D case. The difference between the 2D and 3D

results for printed papers is more muted. This is possibly because while much of the 3D structure of the substrate is obliterated by the laser toner its interaction with the substrate itself (which is evident equally in 2D and 3D) still provides a useful key for classification.

Table 3: Classification results with 3D and 2D information for dataset 2.

Feature	Training	Validation	Test
3D	91.72	95.4	92.55
2D	92.14	92.75	89.36

## 6 CONCLUSIONS

The 3D surface texture presented in this paper shows promising attributes for a measure to be used for accurate and robust classification of paper materials. We presented an ultra-high resolution image sensing device adapted to capture photometric images at a micro-scale level. Using a 4-light source PS approach we have demonstrated that we can recover 3D micro-geometry for different types of paper substrates. Consequently, we show that features extracted from the recovered 3D micro-geometry can be used to characterise and classify different categories of paper types at significantly high-level of accuracy and easily outperforms classification based on features extract from 2D surface information. Additionally the steps involved in deriving the 3D signature have low computational complexity and more importantly is very cost-effective. We believe that a system based on the model presented in this paper can have wide use in several industries where document forgery is a considerable threat.

## REFERENCES

- Adams, G. (2010). Hand held dyson relay lens for anti-counterfeiting. In *Imaging Systems and Techniques (IST), 2010 IEEE International Conference on*, pages 273–278. IEEE.
- Barsky, S. and Petrou, M. (2003). The 4-source photometric stereo technique for three-dimensional surfaces in the presence of highlights and shadows. *Pattern Analysis and Machine Intelligence, IEEE Transactions on*, 25(10):1239–1252.
- Buchanan, J. D. R., Cowburn, R. P., Jausovec, A.-V., Petit, D., Seem, P., Xiong, G., Atkinson, D., Fenton, K., Allwood, D. A., and Bryan, M. T. (2005). Forgery: ‘fingerprinting’ documents and packaging. *Nature*, 436(7050):475.
- Chantler, M., Petrou, M., Penirsche, A., Schmidt, M., and MGunnigle, G. (2005). Classifying surface texture while simultaneously estimating illumination direction. *International Journal of Computer Vision*, 62(1-2):83–96.
- Chiang, P.-J., Khanna, N., Mikkilineni, A., Segovia, M. V. O., Suh, S., Allebach, J., Chiu, G., and Delp, E. (2009). Printer and scanner forensics. *Signal Processing Magazine, IEEE*, 26(2):72–83.
- Clarkson, W., Weyrich, T., Finkelstein, A., Heninger, N., Halderman, J. A., and Felten, E. W. (2009). Fingerprinting blank paper using commodity scanners. In *Security and Privacy, 2009 30th IEEE Symposium on*, pages 301–314. IEEE.
- Cula, O. G. and Dana, K. J. (2001). Recognition methods for 3d textured surfaces. In *Proceedings of SPIE conference on human vision and electronic imaging VI*, volume 4299, pages 209–220.
- Frankot, R. T. and Chellappa, R. (1988). A method for enforcing integrability in shape from shading algorithms. *Pattern Analysis and Machine Intelligence, IEEE Transactions on*, 10(4):439–451.
- Haralick, R. M., Shanmugam, K., and Dinstein, I. H. (1973). Textural features for image classification. *Systems, Man and Cybernetics, IEEE Transactions on*, (6):610–621.
- Johnson, M. K., Cole, F., Raj, A., Adelson, E. H., et al. (2011). Microgeometry capture using an elastomeric sensor. *ACM Trans. Graph.*, 30(4):46.
- Khanna, N. and Delp, E. J. (2010). Intrinsic signatures for scanned documents forensics: effect of font shape and size. In *Circuits and Systems (ISCAS), Proceedings of 2010 IEEE International Symposium on*, pages 3060–3063. IEEE.
- Koenderink, J. J. and van Doorn, A. J. (1992). Surface shape and curvature scales. *Image and vision computing*, 10(8):557–564.
- Kuparinen, T., Kyrki, V., Mielikäinen, J., and Toivanen, P. J. (2007). Paper surface topography using three-light photometric stereo. In *MVA*, pages 45–48. Citeseer.
- Marquardt, D. W. (1963). An algorithm for least-squares estimation of nonlinear parameters. *Journal of the Society for Industrial & Applied Mathematics*, 11(2):431–441.
- McDaniel, T. and Panchanathan, S. (2007). Perceptual surface roughness classification of 3d textures using support vector machines. In *Haptic, Audio and Visual Environments and Games, 2007. HAVE 2007. IEEE International Workshop on*, pages 154–159. IEEE.
- Simske, S. J. and Adams, G. (2010). High-resolution glyph-inspection based security system. In *Acoustics Speech and Signal Processing (ICASSP), 2010 IEEE International Conference on*, pages 1794–1797. IEEE.
- Woodham, R. J. (1980). Photometric method for determining surface orientation from multiple images. *Optical engineering*, 19(1):191139–191139.